Influence of heat treatment conditions on structural and magnetic properties of nickel zinc ferrite nanoparticles synthesized (pH=8) by solution auto combustion method

Richa[1, 2*], A. K. Tyagi[2], D. S. Ahlawat[3], A. Singh[4]

[1]Research Scholar, Department of Physics, I. K. Gujral Punjab Technical University, Kapurthala, 144603, Punjab, India.
[2]Material Research Lab., Department of Applied Sciences and Humanities, Shaheed Bhagat Singh State Technical Campus, Ferozepur 152002, Punjab, India.
[3]Material Science Lab., Department of Physics, Chaudhary Devi Lal University, Sirsa 125055, Haryana, India.
[4]Department of Physics, JCD Memorial (PG) College, Sirsa 125055, Haryana, India.

Abstract

Nickel zinc ferrite nanoparticles were synthesized from metal nitrates precursors via solution auto combustion method, using heat treatment conditions. The crystalline nature of samples was analyzed with X-ray diffraction (XRD) and scanning electron microscopy (SEM). Vibrating sample magnetometer (VSM) was used to study the influence of temperature and heating rate on magnetic properties of nickel zinc ferrite nanoparticles. Samples were made at different temperature 400^oC, 600^oC, 800^oC and 1000^oC with heating rate 10°/min. for 4 hours. Better results were found for sample prepared at 1000^oC. The crystallite size increases from 29.76 nm to 62.26 nm with increase in temperature upto 1000^oC with heating rate 10^oC/min. Our results demonstrate that magnetization of samples modified by enhancement in processing temperature. Highest value of magnetization 72.49e.m.u./g was observed for sample prepared at 1000^oC. Effect of heating rate was also investigated. Sample prepared at 10°/min. heating rate show better results as compared to sample made at 25^oC/min.

1. Introduction

$Ni_{0.5}Zn_{0.5}Fe_2O_4$ (NZF) with the spinel structure draw the attraction of researchers due to its high-resistivity, low-eddy current losses, and is particularly favourable for high-frequency applications. NZF have been used in applications including loading coils, microwave devices, recording heads, antenna rods, and the telecommunication field, drug delivery, sorting, cell labeling, magnetic resonance imaging and therapeutic as well as sensing applications[1-7]. In the typical ion configuration for Ni–Zn bulk ferrites, Ni and Zn ions occupy B-site and A-site positions respectively [8]. The type of cations and their distribution between two interstitial sites in spinel ferrites can be tuned resulting in many interesting properties. The powder preparation methods are: sol–gel methods [9–11], microemulsion [12], hydrothermal-microwave [13], hydrothermal synthesis [14–16], and co-precipitation [17–19]. The solution auto combustion technique has become very popular recently for the preparation of a variety of mixed-metal oxides, nanoporous and nanomaterials oxides due to the high chemical low processing temperatures, homogeneity, and the possibility of controlling the shape and size of particles. It has been observed that the auto combustion method offers considerable advantages such as better mixing of the starting materials and excellent chemical homogeneity in the final material [10]. The properties of such nanoferrites are highly sensitive to the method of preparation, grain size, chemical composition, sintering temperature, atmosphere, type of substituents and the distribution of cations among tetrahedral and octahedral sites.

In the present work, we focus on the properties of NZF powders prepared at different temperatures by a solution auto-combustion technique. The process has the merits of economical precursors, a simple synthesis method, and a resulting nano-sized, homogeneous powder. Research work on nickel zinc ferrites has been reported by various researchers [20-29]. In this paper, we present the magnetic and structural properties of the nanocrystalline NZF powder in relation to the calcination temperature. The observed magnetic behaviour is

Richa et al., J. Mater. Environ. Sci., 2017, 8 (S), pp. 4650-4656

4650

correlated with the average crystallite size of the nanocrystallites were calculated from the x-ray diffraction. The results are then compared with the experimental results obtained by other researchers. Novelty of work is that we have prepared the NZF powder by economical method.

2. Material and Methods

2.1 Materials and methods

Nickel Nitrate Hexahydrate, Zinc Nitrate Hexahydrate, Iron Nitrate Nonahydrate, Citric Acid (Himeida, AR 99%), Ammonia Solution (Sigma Aldrich, 33%). Method used for sample preparation was sol-gel auto combustion method.

2.2 Preparation of ferrite nanoparticles

Powder with a nominal composition of $Ni_{0.5}Zn_{0.5}Fe_2O_4$ was prepared from a mixture of metallic nitrates and citric acid. The materials used were zinc nitrate hexahydrate $Zn(NO_3)_2 6H_2O$, nickel nitrate hexahydrate $Ni(NO_3)_2 6H_2O$, iron nitrate nonahydrate $Fe(NO_3)_3 9H_2O$ [30]. All the metal nitrates were put into stirred double distilled water and increase the temperature of solution upto 100^oC. Citric acid as a fuel was added into continuous stirred metal nitrates solution. The pH value of solution was adjusted to 8 by adding the ammonia solution to stirred solution. After 6-7 hours of continuous of stirring a viscous brown black gel was obtained. Raised the temperature of viscous sol to 250^oC-300^oC and ignition process start with evolution of gases and final product obtained in the form of black brown powder. Ground the as prepared powder (S0)for one hour and heat the powder at temperature 800^oC (S5)with 25^oC/min. for 4 hours. Another series are 400^oC(S1), 600^oC(S2), 800^oC(S3) and 1000^oC(S4) with heating rate of 10°/min.for 4 hours.

2.3 Characterization Techniques

The structural parameters of synthesized NZF were investigated by X-ray diffraction (XRD; The Bruker D8 X-ray diffractometers). The XRD pattern of samples were taken in the angle range 10-80° (2θ) with 2°/min. Magnetic properties of prepared ferrite nanoparticles were studied by a vibrating sampler magnetometer (VSM PAR-155 at IIC, IIT, Roorkee)   Range: 0.00001 to 10000 e.m.u., Magnetic field: 10kOe to +10 kOe , Temperature range : Room Temperature).

3. Results and discussion

3.1 Structural Properties

3.1.1 XRD

The XRD patterns of the prepared samples are demonstrates in Figure1 and Figure 2. The peaks of sample S4 at 18.15^o, 29.95^o, 35.54^o, 36.15^o, 42.60^o, 53.29^o, 56.70^o, 62.30^o corresponding to planes (111), (220), (311), (222), (400), (422), (511), (440) respectively confirms the formation of cubic spinel Structure. Figure 1 shows the XRD pattern of sample prepared at 800^oC with rate 10^oC/min. and 25^oC/min. Figure 2 demonstrates the NZF sample prepared at different temperatures from 400^oC to 1000^oC with heating rate of 10^oC/min. At 1000°C fully crystallized nickel zinc ferrite has formed with sharp peaks. Peaks of the as prepared sample could be attributed to the formation of ferrite particles in nano range. The peak width decreases with the increase of temperature. The sizes of the nanoparticles have been calculated using Scherrer's formula from (311) peak [31]. The crystallite size (D) increases from 29.76 nm to 62.26 nm with the systematic variation of temperature as shown in Table 1. It is expected that if one introduces calcination temperature in the system much higher, the molecular concentration at the crystal surface will increase and hence the crystal growth will be promoted [31]. In addition, a higher temperature can enhance the atomic mobility and make grains get more energy to grow up. The average crystallite size increases slowly from upto 400°C and at temperature 600^oC decrease again and then increase upto 1000^oC. It can seen that intensity of peak corresponding to (311) plane reduced at 600^oC temperature. New phase (o) was formed between (220) and (311) peaks at 600^oC temperature. It clearly shows that at the 600^oC temperature, the sample contains secondary non-magnetic phase. It may be the decomposition of the ferrite into α-Fe_2O_3. Due to this secondary phase, the samples annealed at 600^oC having a low magnetic properties than the other samples in all fuel combustion ratios. These secondary non-magnetic peaks slowly disappeared with increasing the temperature [17]. From the diffraction peak full width at half maximum (β) was Used for calculation of crystallite size (D) of ferrite powder. Here k is structure factor and λ is the wavelength of X-ray.

$$D = \frac{k\lambda}{\beta Cos\theta} \qquad - \qquad (1)$$

$$d = \frac{a}{\sqrt{h^2+k^2+l^2}} \qquad - \qquad (2)$$

Here d, a, and (hkl) represents represent the inter-planar spacing, lattice constant and miller indices respectively. The sample annealed at lower temperature is partially crystallization. So, surface defects can occur within the lattice, but the crystallization will improve with the increase of temperature, which can result in lattice contraction. This increase and decrease of crystallite could be attributed to redistribution of cations between tetrahedral A-site and octahedral B-site and zinc loss from the powder sample [32], respectively.
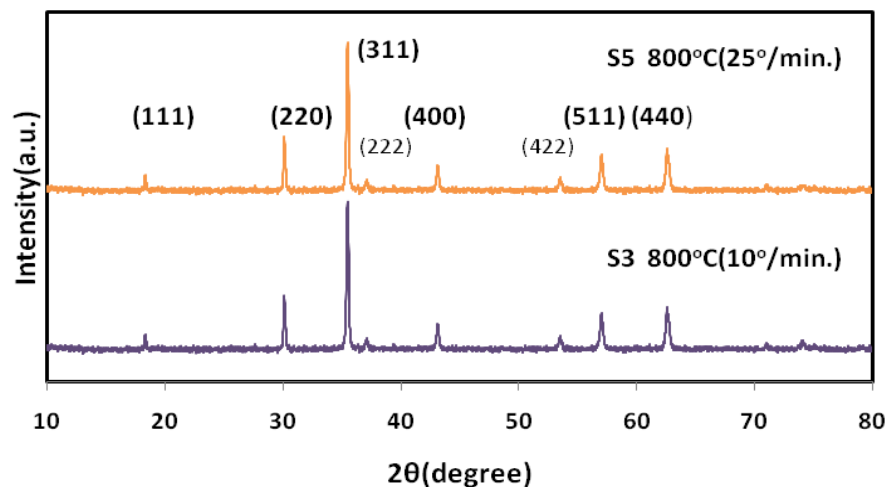

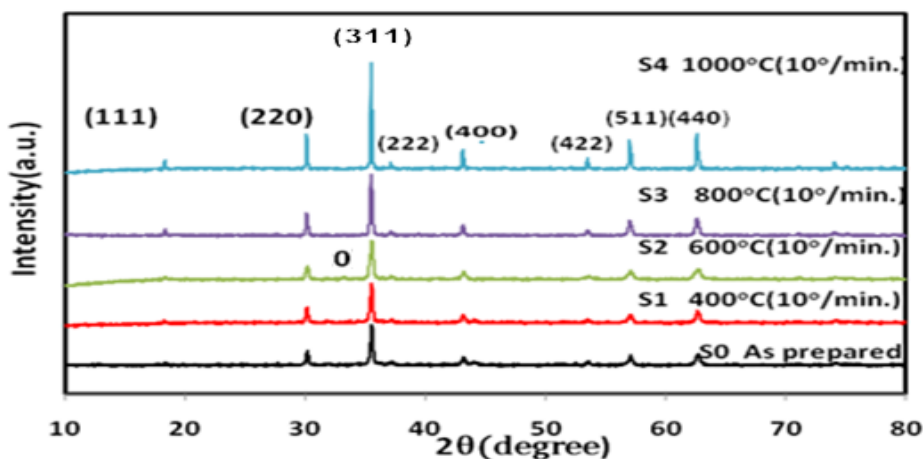Figure1 : XRD Pattern of nickel zinc ferrite prepared at different temperature rate.

Figure2 : XRD Pattern of nickel zinc ferrite prepared at different temperatures.
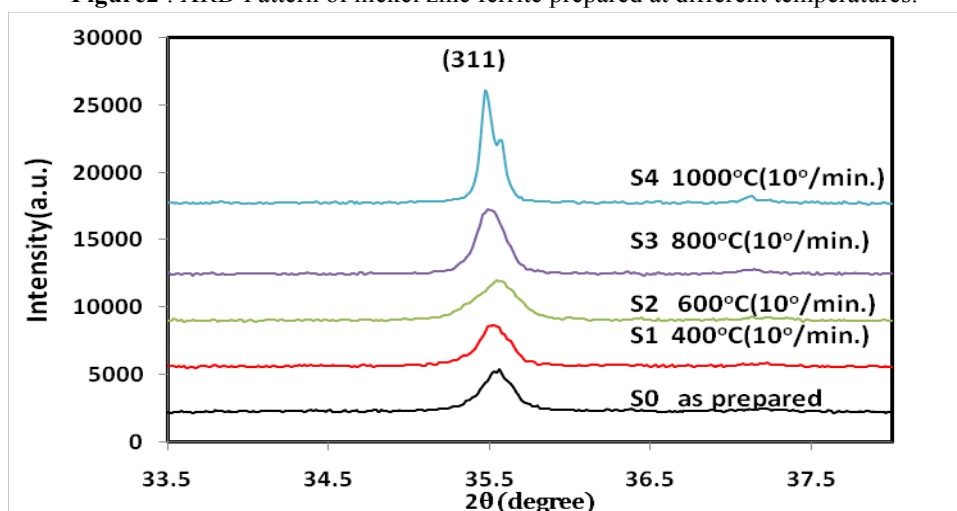

Figure 3 : XRD Peak position (311) of nickel zinc ferrite prepared at different temperatures.

The Lattice parameter (a) was obtained using the powder-diffraction and obtained values are listed in Table 1. [25, 33-35]. Sample S2 shows the different behavior form other samples. Figure 3 represents the variation of peak (311) width with different calcination temperature of samples.

3.1.2 W-H plots

In addition, the Williamson and Hall (W-H) plots are also used to calculate the crystallite size. The strain variation for smaller crystallite which can be due to the increasing defect density. Figure 4 shows the linear fitting W-H plots of S5, S0, S1, S2, S3 and S4. From the diffraction peak full width at half maximum (β) was used for calculation of crystallite size (D) of ferrite powder form W-H equation 3[35].

$$\beta Cos\theta = \mathcal{E}4Sin\theta + \frac{\lambda}{D} \qquad - \qquad (3)$$

Therefore, the calculated crystallite size values were found 36.06 nm, 48.10nm, 42.10 nm, 56.16, 82.5nm, 54.16 for samples S0,S1, S2, S3, S4 and S5 respectively, which are consistent with the previous calculated crystallite size by the Debye-Scherrer equation. So the calcination temperatures play an important role in controlling the crystallite size of the nanocrystallite [34, 36].
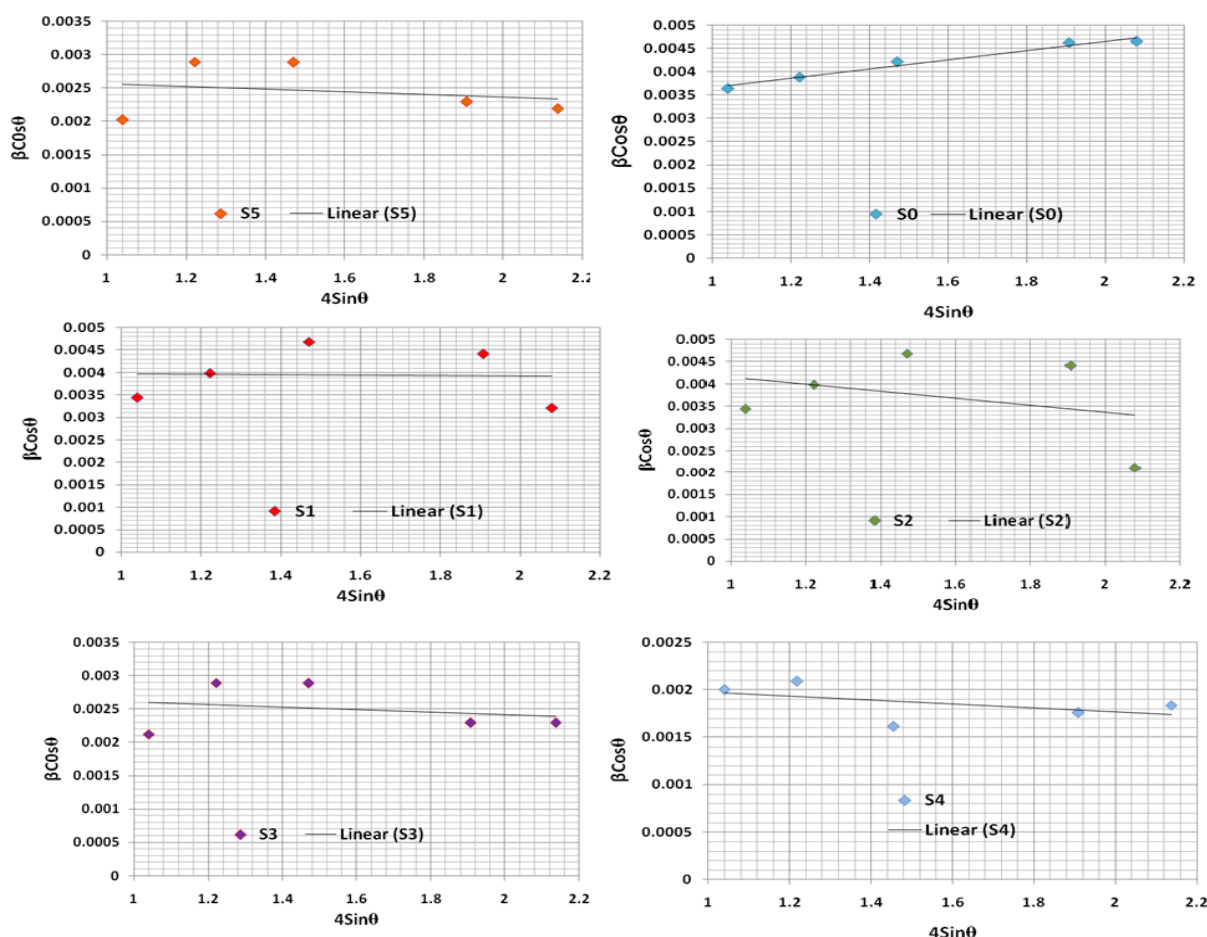

Figure 4: W-H plot of samples prepared at different temperature and heating rate.

Table1: Structural parameters (311) of samples prepared at different temperature and heating rate.

Sample	intensity	d spacing (Å)	Lattice Constant (Å)	Crystallite (311) size-D (nm)	Strain
S0(as prepared)	5394.19	2.5226	8.3665	29.76	0.0030
S1(400°C,10°C/min.)	5321.19	2.5261	8.3780	44.87	0.0026
S2(600°C,10°C/min.)	5238.51	2.5238	8.3704	34.87	0.0034
S3(800°C,10°C/min.)	6996.15	2.5285	8.3860	48.42	0.0025
S4(1000°C,10°C/min.)	10016.12	2.5273	8.3821	62.26	0.0019
S5((800°C,25°C/min.)	6800.23	2.5265	8.3715	45.38	0.0028

3.2 Magnetic Properties

From the VSM data, hysteresis loops are plotted. The variation of saturation magnetization with temperature as demonstrate in the Figure 5 and Figure 6. It can be seen from the Table 2, that the value of saturation

magnetization (M_s) affected by hating rate. Maximum value of M_s was obtained at heating rate of 10°/min as compared to 25^oC/min. With increases in temperature from 400^oC NZF reaches to the low value of 48.88e.m.u./gm for 600^oC temperature and then increase gradually upto 1000^oC as shown in Figure 6. Similar type of behavior was also reported by various researchers [35]. The dependence of saturation magnetization is explained in terms of spin-disorder, crystallite size and spin-canting. In nickel zinc ferrite, the Zn^{2+} ions concentrate preferentially in the A site and the Ni^{2+} ions in B site in cubic spinel lattice [35, 36]. Taking into
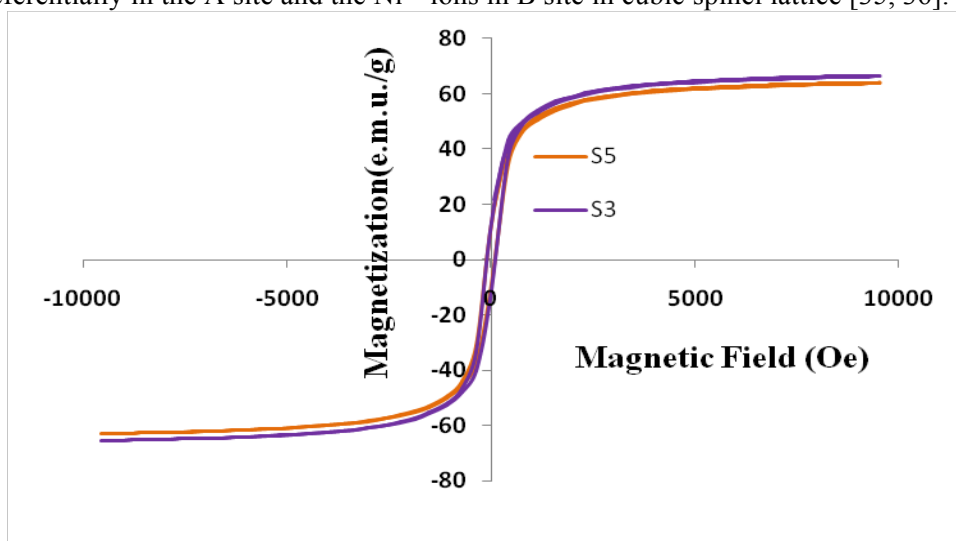

Figure 5 : Plots between magnetization and applied magnetic field of samples prepared at different heating rate.
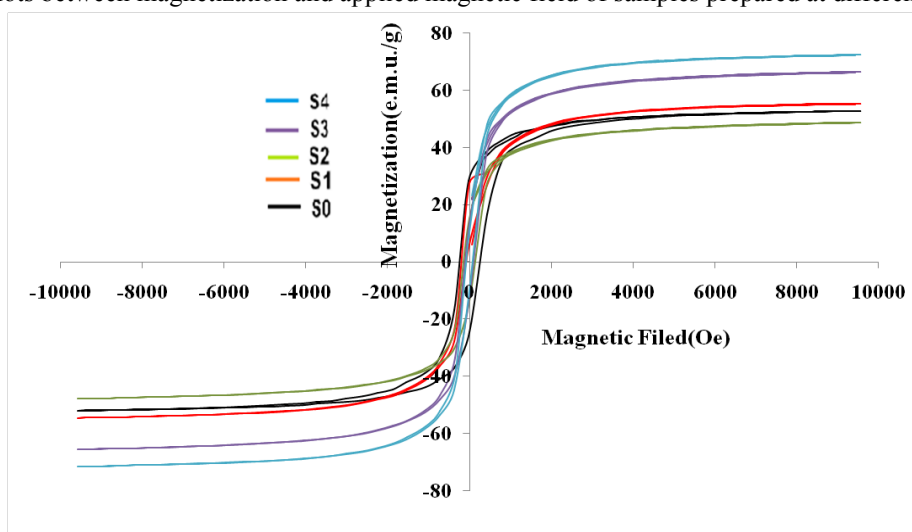

Figure 6 : Plots between magnetization and applied magnetic field of samples prepared at different temperatures.

account that the magnetization of spinel ferrites is given by $M=M_B-M_A$, where M_A and M_B are the magnetization of A and B sites respectively. Generally, for spinel ferrite, the saturation magnetization is influenced by magnetic super exchange interaction of cations between tetrahedral A and octahedral B sites. The iron ions from B-sites are the dominant contributor to the magnetization. At lower temperature, weaker magnetic super exchange interaction and lattice defects can also lead to the smaller value of M_s [37]. Magnetic moment (m) was calculated from formula given in equation 4. Here, M is molecular weight.
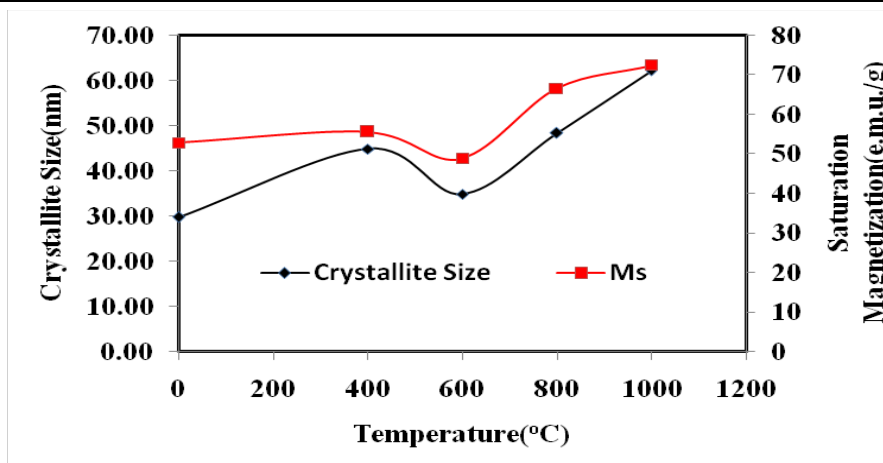
$$m = \frac{M \times M_s}{5585} \qquad - \qquad (4)$$

Magnetic super exchange interaction between the ions increase with increase in temperature. It is seen that saturation magnetization increases as the crystallite size increases. Kumar et al. [38] had investigated that the existence of spin canting, cation distribution, and disordered surface layer could result in decreased in saturation magnetization. The surface effects become significant as the crystallite size increases, which can lead to the increase of M_s. Figure 7 shows the variation of magnetization with crystallite size. Another possible factor is the redistribution of cations between A and B sites, which grows the net magnetic moment. Sreeja et al. [39] had confirmed an abnormal cation distribution of $Ni_{0.5}Zn_{0.5}Fe_2O_4$ with different temperature by Mossbauer
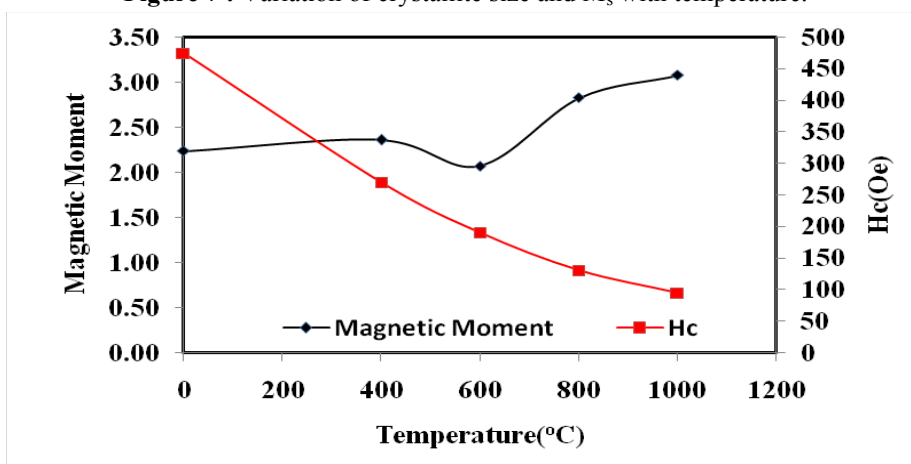
Table 2: Magnetic parameters of NZF samples prepared at different temperature and heating rate.

Samples	Saturation magnetization(M_s) e.m.u./gm	Magnetic moment(Bohr magnetron)	Coercivity (H_c)(Oe)
S0	52.84	2.24	475
S1	55.49	2.36	270.1
S2	48.88	2.07	190.2
S3	66.57	2.83	130.4
S4	72.49	3.08	95
S5	64.16	2.73	128.3

Figure 7 : Variation of crystallite size and M_s with temperature.

Figure 8 : Variation of magnetic moment and H_c with temperature.

Spectroscopic study. From the XRD results, the calcination temperature affects the phase composition of the NZF samples [39]. It clearly shows that at the 600°C temperature, the sample contains some secondary non-magnetic phase. Due to this secondary phase the samples annealed at 600°C (S2) having a low magnetic properties than the other samples. These secondary non-magnetic peaks disappeared with increasing the temperature [40]. The samples S3 and S4 concentration of the secondary phase was reduced. Similar type of behavior was also reported by E. Ranjith et. al.[36]. Due to this reduction, S3 and S4 sample has better magnetic properties than the sample S2 [39]. Variation of magnetic moment and coercivity with temperature shown in Figure 8.

Conclusion
Nanocrystalline nickel zinc ferrite nanoparticles were successfully prepared by solution auto ignition method. The microstructure was studied by XRD, SEM. Magnetic properties were measured with VSM at room temperature. The results showed that uniform and fine ferrites are formed. The crystallite size of sample was found maximum at 1000°C temperature for 4 hours. The saturation magnetization, M_s, of the sample increases with increasing temperature, and the maximum M_s was observed 72.49e.m.u./g. The crystallite size increases

with increase in temperature upto 1000°C with heating rate 10°/min. Our results demonstrate that magnetization of samples is modified by enhancement in temperature and heating rate. Effect of heating rate was also investigated. Sample prepared at 10°/min. show better results as compared to sample made at 25°C/min. heating rate.

References
1. D. Stoppels, *J. Magn. and Mag. Mat.* 160(1998) 323-328.
2. C.O. Robert, Modern magnetic materials principles and application. Beijing: Industry of Chemistry Press (2003).
3. R. Valenzuela, Magnetic Ceramics, Cambridge University Press, Cambridge (1994).
4. F. Bucholtz, Optic Sensors: An Introduction for Engineers and Scientists, John Wiley, New York (1991).
5. A.M. Abdeen, *J. Mang. Magn. Mater.* 185(1998) 199–206.
6. M. Sedlar, L. Pust, *Ceram. Int.* 21(1995) 21-27.
7. Y.W. Bibby, D.C. Larson, Fiber optic magnetic field sensors using metallic glass coated optical fibers, in: Proceedings of the Eighth International Conference on Optical Fiber Sensors, (1992).
8. A. Goldman, *Modern ferrite tech.*. 2nd ed. New York: Springer (2006).
9. J. Azadmanjiri, *Mat. Chem. and Phys*. 109(2008)109-112.
10. S. Zahi, A. Daud, M. Hashi*, Mater. Chem. and Phys.* 106(2007)452-456.
11. K. Wu, T. Ting, M. Li., W. Ho, *J. Mag. and Magnetic Mat*. 298(2006)25-32.
12. C. Liu, B. Zou, A. Rondinone, Z. Zhang, *J. Phys. Chem. B* 104 (2000) 1141-1145.
13. S. Komarneni, M.D. Arrigo, C. Leonelli C., Pellacani, H. Katsuki, *J. Am. Ceramic Soc.* 81 (1998) 3041-43.
14. M. Búcko, K. Haberko., *J. the Euro. Ceramic Soci*. 27(2007)1345-1350.
15. S. Hallynck, G. Pourroy, S. Vilminot, P.M. Jacquart, D. Autissier, N. Vukadinovic, *Solid State Sci.* 8 (2006) 24-30.
16. Z.H. Yang, Z.Q. Gong, H.X. Li, Y.T. Ma, Y.F. Yang, *J. Central South Uni. of Tech*. 61 (2006)8.
17. B. Rao, A. Kumar, H. Rao, Y. Murthy, O. Caltun, I. Dumitru, *J. Optoelec. Advanced Mat.* 8 (2006) 1703-05
18. S. Shenoy, P. Joy, M. Anantharaman, *J. Mag. and Magn. Mat.* 269(2004) 217.
19. W.C. Hsu, S. Chen, P. Kuo, C. Lie, W. Tsai, *Mat. Science and Eng* 111(2004)142-149.
20. J. Schafer, W., Sigmund, *J. Mater. Res.* 12(1997)2518-2521.
21. A. Chakraborty, P. Sujatha, H.S. Devi, *Maiti, Mater. Lett.* 20(1994) 63.
22. Y.K. Sun, S.A. Hong, *J. Mater. Sci.* 31(1996)3617-3621.
23. N. Chakrabarti, H.S. Maiti, *Mater. Lett*. 30(1997)169-173.
24. S. Torkian, A. Ghasemi, R. Shoja, Razavi, M. Tavoosi, *J. Supercond. and Novel Mag.* 29(2016)1627-1640.
25. M. Kurian, D.S. Nair, *J. of Saudi Chem. Soc*. 20(2016)517-522.
26. S.M. Rathod, V.G. Deonikar, P.P. Mirage, *Adv. Sci. Lett.* 22 (2016) 964.
27. R.B. Bhise, V. Bhong, S.M. Rathod, *Bionano Front.* 8 (2015)107-109.
28. Y.K. Dasan, B.H. Guan, M.H. Zahari, L.K. Chuan, *PLOS One* 12(2017)170075.
29. Richa, A.K. Tyagi, D.S. Ahlawat, *Orient. J. Chem*. 33(2017)296-303.
30. N. Lwin, R. Othman, A.M. Noor, S. Sreekantan, T.C. Yong, R. Singh, C.C. Tin, *Mat. Characte.* 110 (2015) 109-115.
31. C. Upadhyay, H.C. Verma, S. Anand, *J. Appl. Phys.* 95, (2004) 5746–5751.
32. Sutka, K. A. Gross, G. Mezinskis, G. Bebris, M. Knite, *Physica Scripta* 83(2011)025601.
33. M. Zhang, Z. Zhenfa, L. Qiangchun, Z. Peng, T. Xianwu, Y. Jie, Z. Xuebin, S. Yuping, D. Jianming, *Advances in Mat. Science and Eng.* 1(2013)10.
34. D. Venkatesh, M.S.R. Prasad, B.R. Babu, K.V. Ramesh , K. Trinath, *J. Magn.* 20 (2015)229-240.
35. E.R. Kumar, R. Jayaprakash, *J. of Mag. and Mag. Mat*. 348(2013) 93–100.
36. G.K. Williamson, W.H. Hall, *Acta Metall.* 1(1953) 22-31.
37. A. Kumar, A. Annveer, M. Arora, M.S. Yadav, R.P. Pant R.P, *Phys. Proc.* 9(2010) 20–23.
38. S. Kumar, V. Singh, S. Aggarwal, U.K. Mandal, R.K. Kotnala, *Mat. Sci. and Eng. B*, 166 (2010)76–82.
39. V. Sreeja, S. Vijayanand, S. Deka, P.A. Joy, *Hyperfine Interactions* 183(2008)99–107.
40. P. Hu, H. Yang, D. Pan, H. Wang, J.J. Tian , S. Zhang , X. Wang, A.A. Volinsky, *J. Magn. and Mag. Mat.* 322(2010)173.

(2017); http://www.jmaterenvironsci.com